MARS ENTRY, DESCENT, AND LANDING RECONSTRUCTION FROM FLIGHT DATA: UNCERTAINTY QUANTIFICATION

Bart Van Hove[(1)], Özgür Karatekin[(2)]

[(1)]Royal Observatory of Belgium, Ringlaan 3, 1000 Brussel, Belgium, Email:bartvh@observatory.be
[(2)]Royal Observatory of Belgium, Email:o.karatekin@observatory.be

ABSTRACT

Five spacecraft successfully performed entry, descent and landing (EDL) on Mars in the past two decades. Post-flight reconstruction from flight data provides input for design margins and, especially in the case of atmospheric reconstruction, allows in-situ atmospheric science investigation of the Martian environment. The present work deals with uncertainty quantification (UQ) and considers both stochastic sampling (Monte Carlo) and Bayesian state estimation (Kalman filter). The consequences for UQ of accelerometer and gyroscope noise properties such as cross-correlation, Gaussianity and frequency content are assessed in a case study of the 2008 Phoenix reconstruction. White noise assumptions are shown to potentially overestimate reconstruction uncertainty bounds, both in Monte Carlo approaches and our preliminary Kalman filter implementation. This work was performed in preparation for the 2016 ESA ExoMars science investigation.

1. INTRODUCTION

Mars atmospheric entries are performed autonomously in a poorly known environment compared to Earth's. Entry velocities typically in excess of 5 km/s are reduced mainly by aerodynamic drag. Entry system design requires predictions of atmospheric conditions and vehicle aerothermodynamics. Entry system design relies on wind tunnel testing, computational fluid dynamics (CFD) and atmospheric models. Comparison to flight is necessary to validate these tools and reduce uncertainty bounds on their predictions. To improve landing precision, maintain robustness while reducing design margins and to implement new flight technologies, post-flight reconstruction is essential. Reconstruction of the flown trajectory and atmospheric environment has been carried out for every Mars lander [1,2,3,4,5]. Accurate uncertainty bounds on those flight reconstructions are required for their interpretation.

While the above engineering objectives drive in-flight data recording, scientific studies can utilize these measurements as well. Large scale oscillations of atmospheric temperature consistent with thermal tides were observed in a Phoenix reconstruction [6]. Pathfinder's reconstruction suggested the presence of CO_2 clouds, indeed confirmed later by observations from the landed platform [7,8]. Flight data from instrumented heat shields on future landers may be able to constrain wind profiles [9] at altitudes for which no such observations currently exist. Scientific conclusions drawn from flight data require accurately determined uncertainty bounds.

In the present study we first characterize sensor noise in the 2008 Phoenix inertial flight measurement dataset. We then evaluate the modelling specific noise properties such as cross-correlation and frequency content for reconstruction UQ. First, two common Monte Carlo sampling approaches are compared. We then address the same question for a non-linear Kalman filter.

2. CONVENTIONAL RECONSTRUCTION METHODOLOGY USING IMU DATA

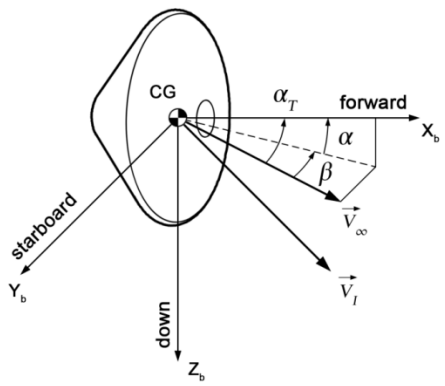

Fig. 1. Vehicle carried body frame with inertial and relative velocity vectors and flow angles

2.1 Flight data preparation

An Inertial Measurement Unit (IMU) is a package of accelerometers and gyroscopes that measures linear acceleration and angular rotation rates. Phoenix recorded six degrees of freedom (6-DOF) inertial rates at 200 Hz throughout the entire EDL. The current work uses the freely available raw IMU dataset [10] corrected for bias offsets and divided by $\Delta t = 0.005$ s to convert velocity and angular increments to rates.

Figure 1 describes the body coordinate frame aligned with the Phoenix geometry and with its origin on the center of gravity. We refer to the body frame with indices *x*, *y* and *z*. Inertial and atmosphere relative velocity vectors are distinct. Angle of attack α, side slip angle β and total angle of attack α_T express the atmosphere relative velocity direction relative to the body frame.

The IMU data was transformed to the body frame from the local IMU frame using the transformation matrix given in [11]. Next, smoothing methods were selected to eliminate noise while avoiding artefacts such as smoothing bias. For the gyroscope data this was achieved with a 64 point moving window 2nd order polynomial fit.

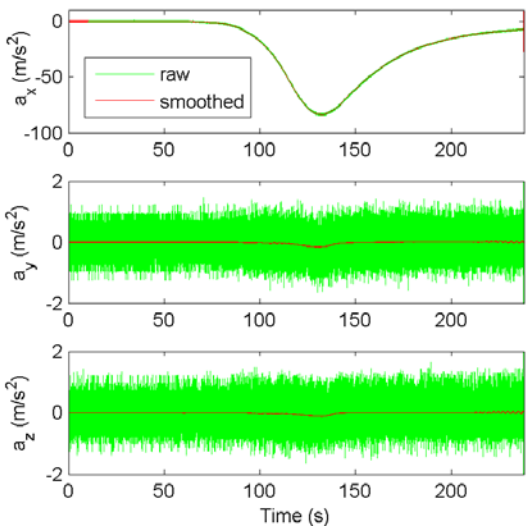

Fig. 2. Body frame IMU acceleration flight data

Axial acceleration was smoothed using a custom method presented in [11]. Axial acceleration increases nearly exponentially before peak deceleration. The arithmetic mean of an exponential signal is not equal to the center value of the window considered, causing moving average smoothers to introduce a bias. This smoothing method eliminates that bias by combining moving average results obtained with different window sizes. Normal acceleration components exhibit no exponential rise and were smoothed with a 255 point moving average. Smoothed body frame acceleration data is shown in Figure 2, the data noise will be defined later as the raw data subtracted by these smoothed signals.

2.1 Trajectory reconstruction

From an initial state provided by [10] at approximately 130 km altitude, smoothed accelerations and rotation rates were integrated with a 4th order Runge-Kutta routine. This provides the inertial flight trajectory of Phoenix up to parachute deployment. Other quantities including relative velocity, angle of attack and altitude above ground can be derived. Trajectory reconstruction is described in more detail in [12,13].

2.2 Atmospheric reconstruction

In a second step, atmospheric profiles are derived from the trajectory. Atmospheric density is commonly estimated from the drag equation [11-14]. In Eq. 1, this equation is arranged to calculate atmospheric density as a function of measured deceleration:

$$\rho_\infty(h) = 2\frac{m \cdot |\vec{a}|}{C_D \cdot A_{ref} \cdot |\vec{V}_\infty|^2} \tag{1}$$

$\boldsymbol{\rho_\infty(h)}$ is the density profile versus altitude $\boldsymbol{h}$, $|\vec{\boldsymbol{a}}|$ the aerodynamic acceleration magnitude, $\boldsymbol{C_D}$ the non-dimensional aerodynamic drag coefficient, $|\vec{\boldsymbol{V}}_\infty|$ the air speed, $\boldsymbol{m}$ the vehicle mass and $\boldsymbol{A_{ref}}$ the reference surface area based on the heat shield radius. Note that $\boldsymbol{C_D}$ is the *predicted* aerodynamic drag and cannot be constrained by IMU flight data. Any drag coefficient uncertainty is propagated directly to the reconstructed atmospheric density. In [14] the 3-σ uncertainty on $\boldsymbol{C_D}$ for Phoenix was estimated at ±3% above Mach 10 and ±10% below Mach 5.

Additional atmospheric profiles are derived from the density profile in two steps. First in Eq. 2, atmospheric pressure $\boldsymbol{p_\infty(h)}$ is estimated by integrating density over altitude according to hydrostatic equilibrium. Second in Eq. 3, density and pressure are combined in the ideal gas law to derive atmospheric temperature $\boldsymbol{T_\infty(h)}$

$$p_\infty(h) = p_\infty(h_0) - \int_{h_0}^{h} g \cdot \rho_\infty \cdot dh \tag{2}$$

$$T_\infty(h) = \frac{\mu \cdot p_\infty}{R \cdot \rho_\infty} \tag{3}$$

with gravitational acceleration $\boldsymbol{g}$, ideal gas constant $\boldsymbol{R}$ = 8.3144621 J/mol/K and molecular weight $\boldsymbol{\mu}$ of the atmospheric gas. $\boldsymbol{\mu}$ and $\boldsymbol{g}$ vary slightly with altitude.

Eq. 3 also requires a pressure boundary condition $\boldsymbol{p}_\infty(\boldsymbol{h_0})$ that was estimated by [11] for the high altitude initial trajectory state.

3. PHOENIX IMU DATA NOISE ANALYSIS

3.1 Noise characterization

We define noise as the data removed by smoothing as described in Section 2. The objective is to construct a description of the IMU data noise for UQ approaches to use in the next sections. All noise was found to be distributed normally as illustrated by the gyroscope noise probability density function (PDF) in Figure 3, but also every other noise signal.

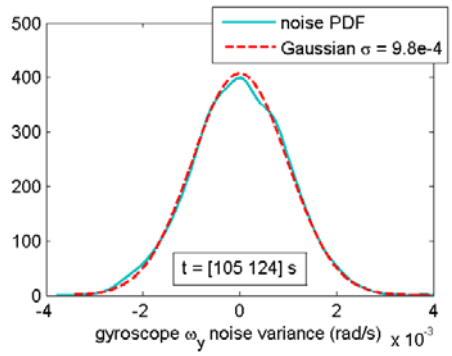

Fig. 3. PDF of noise in gyroscope rotation rate ω_y compared to Gaussian fit (normal distribution)

Cross-correlations exist between the three spatial components of the accelerometer and gyroscope noise, as well as between accelerometer and gyroscope components. Figure 4 is a scatter plot of the axial a_x and normal a_y acceleration noise, including the eigenvectors of the covariance matrix between them. Perfectly horizontal and vertical eigenvectors indicate zero correlation, whereas the rotated noise cloud corresponds to a linear correlation coefficient [15] of about 0.35, normalized so that +1 equals total positive correlation. Cross-correlations exist between all noise signals, varying over time and bounded by ±0.40.

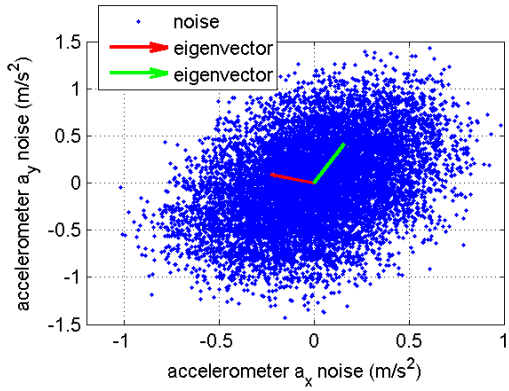

Fig. 4. Scatter plot of cross-correlated noise in two accelerometer components, including covariance matrix eigenvectors

Figure 5 shows the power spectral density (PSD) of the ω_x gyroscope noise and of the a_x acceleration noise. These PSD are also representative of the y and z acceleration and angular rate measurements. The IMU noise is contains relatively high frequencies. Sharply defined power peaks at 16 and 32 Hz for the gyroscopes, also 76 Hz for the accelerometers, may be digitization artefacts or mechanical resonance frequencies. However the main feature of these power spectra is limited frequency content below 50 Hz. We refer to these frequency distributions as *colored noise*.

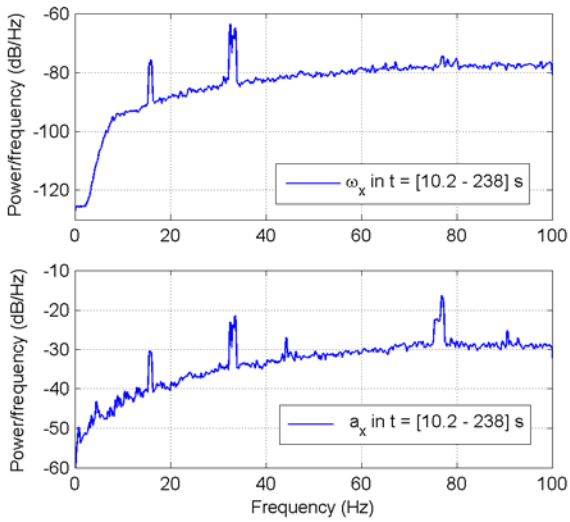

Fig. 5. Power spectral densities (PSD) of IMU data noise in gyroscope rotation rate ω_x (rad/s) and accelerometer velocity rate a_x (m/s^2)

3.2 Noise description

We confirmed that the normal distribution and the power spectral density are stationary properties of the IMU noise, meaning they vary only slightly from entry

interface up to parachute deployment. On the other hand, cross-correlations vary over time. A noise description was constructed that consists of

- Frequency dependent PSD per IMU signal.
- One 6-by-6 covariance matrix with variances for diagonal elements co-variance for off-diagonal elements.
- Co-variances are represented by 2nd order polynomial functions of time

This description is practical for noise generation routines to use. We verified that those successfully generate noise with the characteristics just described. Table 1 lists the matrix diagonal elements, i.e. the Gaussian noise variance for every IMU signal.

Tab. 1. Variance σ^2 of IMU data noise during entry

IMU	noise variance $(m/s^2)^2$	IMU	noise variance $(rad/s)^2$
a_x	0.103	ω_x	1.21e-6
a_y	0.225	ω_y	1.00e-6
a_z	0.253	ω_z	0.90e-6

4. UNCERTAINTY QUANTIFICATION: MONTE CARLO SAMPLING

Monte Carlo sampling aims to approximate probability density functions (PDF) of calculation results, given the PDF of uncertain data inputs and parameters. For reconstruction, these are initial trajectory state uncertainty, IMU data noise and parameter uncertainty such as on the drag coefficient. By sampling inputs and calculating outputs N times, the resulting output samples tend to the output PDF for large N. While computationally expensive, Monte Carlo works for uncertainty descriptions and calculation routines of arbitrary complexity and form.

Therefore we can choose to sample data noise using co-variances and frequency content (PSD) to generate *cross-correlated colored noise* for comparison with the common *uncorrelated white noise* assumption. Two distinct approaches were furthermore compared:

for every of N Monte Carlo realizations:

A) Generate and apply raw data noise before smoothing

B) Generate and apply post-smoothing noise (without smoothing)

Both approaches start from the smoothed IMU data obtained in Section 2. Approach A) is conceptually simple in that it runs through the entire reconstruction process including data smoothing for every Monte Carlo realization. Approach B) may be less expensive computationally, but its equivalence to A) requires an accurate description of the post-smoothing noise. The noise description constructed before is appropriate only for approach A), post-smoothing noise estimation is discussed below.

4.1 Input uncertainty

Figure 6 shows the 3-σ bound[1] on the axial acceleration noise entering into the reconstruction, i.e. also for approach A) this represents the noise variance after smoothing. Every Monte Carlo was verified to have converged numerically, requiring $N \geq 1000$ to 2000. These results are compared to a similar Monte Carlo analysis in the Phoenix IMU reduced dataset published on the Planetary Data System (PDS) [11].

Cross-correlations had negligible impact and are not considered further. However, assuming white noise in approach A) significantly overestimated the acceleration noise. The smoothing methods perform less well for the generated white noise than for the real noise. By comparison, generated colored noise was smoothed out much better. Generating raw data noise in the Monte Carlo thus requires modelling the frequency content.

For approach B), generating post-smoothing noise requires a different noise description. We used the variance of the post-smoothing noise obtained by A) with colored noise generation, but assumed this post-smoothing noise to be white. Naturally the variance for approach B) in Figure 6 matches that of its definition A) with colored noise. The impact of the white noise assumption for B) is assessed below.

[1] three times the standard deviation or square root of the variances such as those listed in Table 1

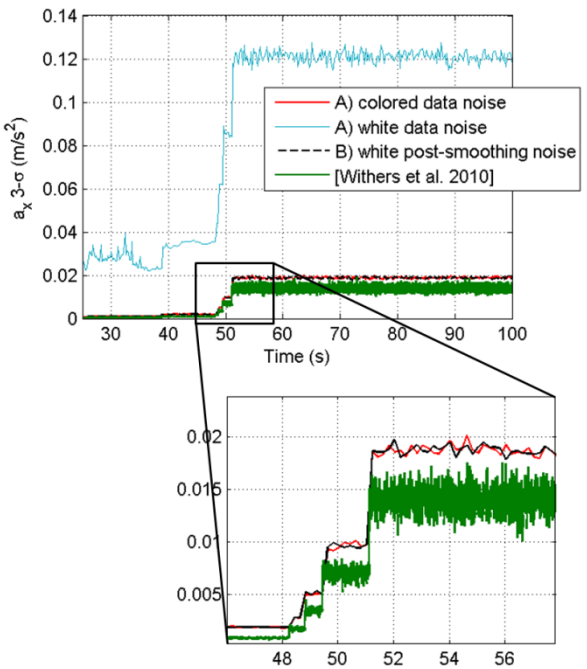

Fig. 6. IMU axial acceleration data input 3-σ uncertainty in Monte Carlo's

Post-smoothing noise variance on PDS was calculated with an empirical formula, and is close to but slightly smaller than our colored noise Monte Carlo estimate. Conversely, normal acceleration to which the above conclusions also apply, have higher variance on PDS. Normal components are of secondary importance given their small magnitude (see Figure 2).

4.2 Reconstruction output uncertainty

Thus far we have discussed data input uncertainty. Now we present the resulting uncertainty bounds on reconstruction outputs. Figures 7 and 8 indicate that assuming white input noise may lead to significantly overestimated reconstruction uncertainty. Parachute opening altitude is reconstructed with over five times the confidence by taking into account noise frequency content. Uncertainty bounds on PDS correspond better with the overestimates and did assume white noise.

Quantities such as angle of attack and altitude are primarily calculated from IMU data, whereas atmospheric density and derived atmospheric profiles rely also on the predicted drag coefficient. White noise assumptions had negligible impact on atmospheric profile uncertainty. Atmospheric reconstruction was based on measured acceleration and estimated drag coefficients: uncertainty of the latter significantly outweighed that on IMU measurements.

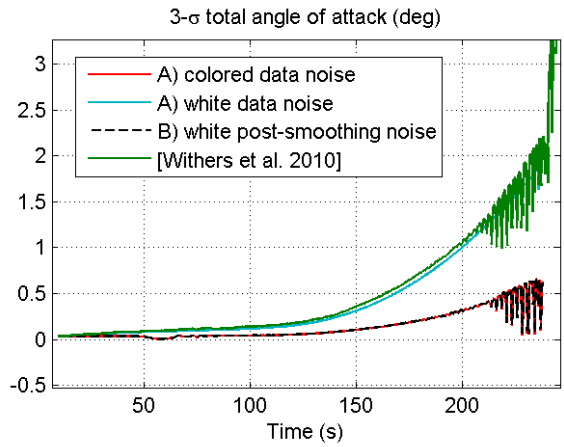

Fig. 7. Monte Carlo 3-σ uncertainties on reconstructed total angle of attack

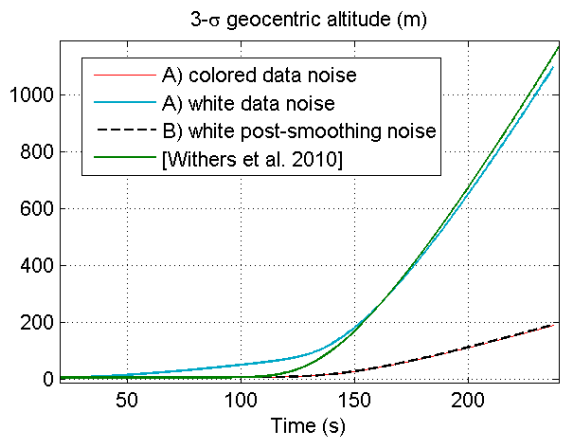

Fig. 8. Monte Carlo 3-σ uncertainties on reconstructed altitude

Although the post-smoothing noise for B) was assumed white, the resulting reconstruction uncertainty almost exactly matches A) with colored noise. This could be exploited to marginally speed up the Monte Carlo. However, since post-smoothing variance was estimated by going through the process of generating raw data noise and analysing the smoothed results, we prefer A) and include those steps in the Monte Carlo analysis.

The PDS Monte Carlo results contain an apparent contradiction between low input uncertainty (Figure 6) and high output uncertainty (Figures 7-8). Results in the next section suggest that in [11], gyroscope noise was overestimated similar to the A) with white noise approach. Gyroscope noise is not described in great detail in [11], so currently we have not verified this conclusively.

5. UNCERTAINTY QUANTIFICATION: KALMAN FILTERING

Bayesian state estimation, of which Kalman filters are a particular implementation, is a different approach to EDL reconstruction and uncertainty quantification. State estimators operate on unsmoothed data and employ predictive models of both measurements (IMU data) and states (trajectory, atmosphere…) to calculate a state estimate with associated uncertainty bounds. Kalman filters are computationally cheaper than Monte Carlo sampling and while using similar equations, completely replace the conventional deterministic methodology presented in Section 2.

5.1 Theory of recursive state estimation

Consider the state vector $\boldsymbol{x}$ that describes a system under consideration. In this case it includes kinematic trajectory characteristics such as position and velocity, and atmospheric conditions such as density. The measurement vector $\boldsymbol{z}$ holds observations: unsmoothed IMU data.

First, the state estimator's *prediction stage* employs state propagation models (flight equations, atmospheric models) and measurement models that predict observations given some state. Second, the *update stage* confronts these predictions with the actual observations to infer a final estimate of the state probability density function (PDF). The update operation is based on the recursive Bayes' rule in Eq. 4 and is carried out for subsequent discrete time intervals distinguished by index *k*.

$$P(x_k|z_k) \sim P(z_k|x_k) \cdot P(x_k|z_{k-1}) \tag{4}$$

PDF in Eq. 4 denoted by $\boldsymbol{P}(\cdot)$ from right to left:

$P(x_k\|z_{k-1})$	**prior state estimate** from a *prediction stage* where current measurement $\boldsymbol{z_k}$ is not used yet
$P(z_k\|x_k)$	**observation likelihood** represents the *update stage* that incorporates the measurement $\boldsymbol{z_k}$
$P(x_k\|z_k)$	**final state estimate** $\boldsymbol{x_k}$ given or 'conditional on' measurements $\boldsymbol{z_k}$

The prediction term can be expanded to reveal the previous final state estimate $\boldsymbol{x_{k-1}}$ and state propagation model. More complete introductions are presented in [16,17,18]. For the present work we highlight these key features of Bayesian state estimation:

- Calculates and propagates PDF
- Blends prediction with observation
- May combine multiple measurement sets
- General but abstract mathematical framework: practical implementations require simplification or approximation

Combining multiple measurement sets is the main motivation for the current development of these methods for Mars EDL reconstruction [5,19]. Recent landers such as Mars Science Laboratory and ExoMars carry instrumented heat shields. State estimators are used to mix in those complementary observations of flow angles and atmospheric conditions.

The issue of implementation has spurred development of dozens of filtering algorithms. The original Kalman filter [20] is an exact analytical solution but only for linear, Gaussian white noise state estimation problems. Other varieties of Kalman filters that can deal with non-linear models such as flight equations, or more complex PDF such as non-Gaussian and colored noise distributions, are approximate solutions[2].

5.2 UKF implementation

The Kalman filter variety used here is the Unscented Kalman filter (UKF) that owes its name to 'unscented transformations' which propagate Gaussian probability densities through non-linear equations. Our UKF algorithm closely resembles that of [21].

Blending prediction and observation is different from conventional reconstruction methodology and requires predictive models. These are constructed from flight equations and atmospheric models. However there is no unique or conventional formulation of EDL reconstruction as a state estimation problem. The detailed design of state and observation models is not necessarily clear-cut, and appropriate uncertainties must to be attributed to them. An optimal formulation is the subject of future work and beyond the scope of this text. Our preliminary formulation is based on that of [5] but considers only IMU flight data.

5.3 Preliminary UKF results

Recalling the impact of white input noise in the Monte Carlo approaches, we now address the same question for the Kalman filter. The UKF uses unsmoothed IMU data and a data noise description composed only of the variances in Table 1. This implies uncorrelated white Gaussian noise.

---

[2] approximation can be negligible but also difficult to quantify, it may also cause numerical instability

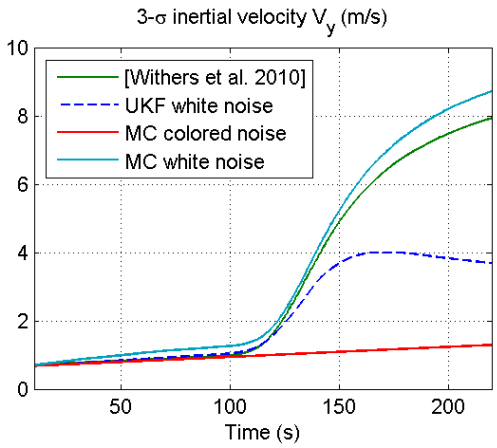

Fig. 9. Kalman filter (UKF) & Monte Carlo (MC) uncertainty bound on reconstructed inertial velocity V_y in planet centered coordinates

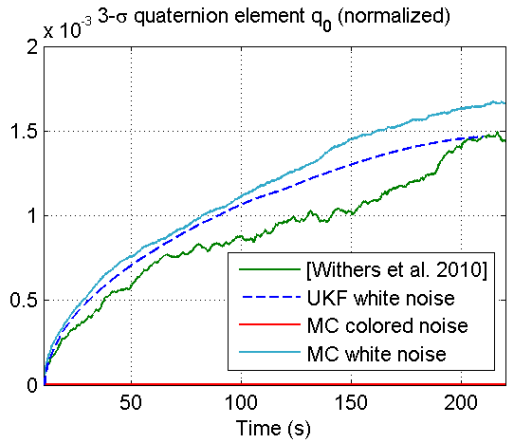

Fig. 10. Kalman filter (UKF) & Monte Carlo (MC) uncertainty bound on reconstructed vehicle attitude (single quaternion component q_0)

Figure 9 shows the 3-σ bound on reconstructed inertial velocity that is mainly dependent on IMU data. The UKF predicts larger uncertainties than the Monte Carlo approach with colored noise and is more similar to the white noise overestimation and PDS results. These results suggest that perhaps by a smaller but significant amount, neglecting IMU data noise frequency content affects Kalman filters similarly as demonstrated by Monte Carlo before.

Figure 10 shows similar results for one of four quaternion components that describe vehicle attitude. This quantity depends exclusively on gyroscope data. Uncertainty estimates from the UKF, Monte Carlo with white noise and PDS all match closely but overestimate compared to the Monte Carlo with colored noise bounds, which is much smaller but non-zero. Strong dependence of the quaternion on gyroscope data suggests that PDS gyroscope noise was overestimated consistently with white noise assumptions.

Figure 11 confirms that as stated before, atmospheric reconstruction uncertainty is insensitive to IMU white noise assumptions. Atmospheric pressure and temperature are derived from the density profile and exhibit the same characteristic.

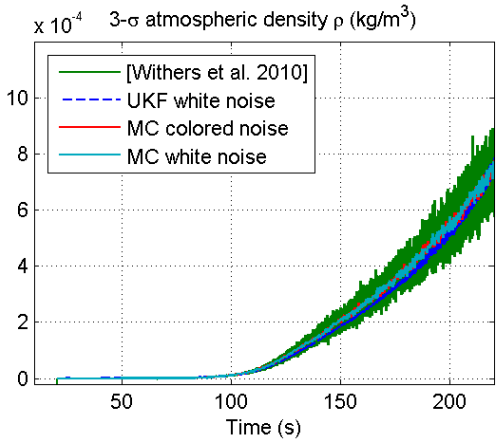

Fig. 11. Kalman filter (UKF) & Monte Carlo (MC) uncertainty bound on reconstructed atmospheric density

6. CONCLUSIONS

Mars EDL reconstruction UQ was carried out for the entry phase using both Monte Carlo sampling and an Unscented Kalman filter. Raw accelerometer and gyroscope data from the Phoenix entry was found to contain Gaussian, cross-correlated, colored noise. Monte Carlo analyses indicated that IMU noise frequency content, including its effect on smoothing, should be evaluated carefully to calculate uncertainty bounds on trajectory reconstructions. When white noise assumptions were not justified, they overestimated reconstruction uncertainty which in most cases is conservative. Atmospheric reconstruction was almost insensitive to these assumptions. Neglecting cross-correlations had no significant impact.

Preliminary results from the UKF suggest that these conclusions also apply to Bayesian state estimators. Future work will compare alternative formulations of EDL reconstruction as a Bayesian estimation problem, and assess the potential benefit of colored noise models for Kalman filters.

REFERENCES

[1] E. A. Euler et al., *Design and Reconstruction of the Viking Lander Descent Trajectories*, J. Guidance and Control, Vol. 1, No. 5, pp. 372-387, 1978.

[2] D. A. Spencer, R. C. Blanchard et al., *Mars Pathfinder Atmospheric Entry Reconstruction*, AAS/AIAA Space Flight Mechanics Meeting, AAS 98-146, Monterey, California, 9-11 February, 1998.

[3] P. N Desai & P. C. Knocke, *Mars Exploration Rovers Entry, Descent, and Landing Trajectory Analysis*, J. of the Astronautical Sciences, Vol. 55, No. 3, pp. 311-323, July-September, 2007.

[4] R. C. Blanchard & P. N. Desai, *Mars Phoenix Entry, Descent, and Landing Trajectory*, J. of Spacecraft and Rockets, Vol. 48, No. 5, September-October, pp. 809-821, 2011.

[5] C. D. Karlgaard et al., *Mars Science Laboratory Entry, Descent, and Landing Trajectory and Atmosphere Reconstruction*, 23rd AAS/AIAA Space Flight Mechanics Meeting, AAS 13-307, 10-14 February, Kauai, HI, USA, 2013.

[6] P. Withers & D. C. Catling, *Observations of atmospheric tides on Mars at the season and latitude of the Phoenix atmospheric entry*, Geophys. Res. Letters, Vol. 37, L24204, 2010.

[7] J. T. Schofield et al., *The Mars Pathfinder Atmospheric Structure Investigation/Meteorology Experiment (ASI/MET)*, Science, 278, pp. 1752-1758, 1997

[8] R. T. Clancy & B. J. Sandor, *CO_2 ice clouds in the upper atmosphere of Mars*, Geophys. Res. Letters, Vol. 25, No. 4, pp. 489-492, 1998.

[9] B. Van Hove & Ö. Karatekin, *Observing the Martian Atmosphere Using Entry Probe Flight Instrumentation*, 5th International Workshop on Mars Atmosphere: Modelling and Observations, 13-16 January, Oxford University, Oxford, UK, 2014.

[10] L. F. Huber, *Atmospheric Structure Experiment (ASE) Data Archive (PHX-M-ASE-2-EDL-V1.0)*, Planetary Data System (PDS), published 2008. `http://atmos.nmsu.edu/PDS/data/phxase_0001/`

[11] J. R. Murphy et al., *Phoenix Atmospheric Structure Experiment Archive (PHX-M-ASE-5-EDL-RDR-V1.0)*, Planetary Data System (PDS), published 2010. `http://atmos.nmsu.edu/PDS/data/phxase_0002/`

[12] B. Van Hove & Ö. Karatekin, *Mars Atmosphere Reconstruction using a Flush Air Data System on the ExoMars Entry, Descent and Landing Demonstrator Module*, 10th International Planetary Probe Workshop, 17-21 June, San Jose, CA, USA, 2013.

[13] P. Withers et al., *Analysis of entry accelerometer data: A case study of Mars Pathfinder*, Planetary and Space Science, Vol. 51, pp. 541-561, 2003.

[14] K. T. Edquist, et al., *Aerodynamics for Mars Phoenix Entry Capsule*, J. of Spacecraft and Rockets, Vol. 48, No. 5, pp. 713–726, 2011.

[15] D. C. LeBlanc, *Statistics: Concepts and Applications for Science, Volume 2*, Jones & Bartlett Learning, pp. 292-299 Ch. 13.1 Correlation Analysis, 2004.

[16] B. Ristic, S. Arulampalam, N. Gordon, *Beyond the Kalman filter*, Artech House, Boston/London, 2004.

[17] D. Simon, *Optimal State Estimation (Kalman, H-infinity and Nonlinear Approaches)*, John Wiley & Sons Inc., 2006.

[18] D. Salmond & N. Gordon, *An introduction to particle filters*, September 2005 (incomplete draft).

[19] S. Dutta, *Statistical methods for Reconstruction of Entry, Descent, and Landing Performance with Application to Vehicle Design*, PhD thesis, Georgia Institute of Technology, December 2013.

[20] R. E. Kalman, *A New Approach to Linear Filtering and Prediction Problems*, Transactions of the ASME - Journal of Basic Engineering, Vol. 82, Series D, pp. 35-45, 1960.

[21] R. van der Merwe & E. A. Wan, *Sigma-Point Kalman filters for Integrated Navigation*, Proceedings of the 60th Annual Meeting of The Institute of Navigation (ION), Dayton, Ohio, USA, pp. 641-654, 2004.